

## Supplementary Information

### A Conjugated Tetracarboxylate Anode for Stable and Sustainable Na-ion Batteries

Kaiqiang Qin,<sup>a</sup> Kathryn Holguin,<sup>a</sup> Motahareh Mohammadiroudbari,<sup>a</sup> Chao Luo<sup>\*a,b</sup>

<sup>a</sup>Department of Chemistry and Biochemistry, George Mason University, Fairfax, VA, 22030, USA

<sup>b</sup>Quantum Science & Engineering Center, George Mason University, Fairfax, VA, 22030, USA

\*To whom correspondence should be addressed. E-mail: [cluo@gmu.edu](mailto:cluo@gmu.edu)

#### *Author contributions*

Kaiqiang Qin: Conceptualization, Data curation, Investigation, Methodology, Visualization, Writing – review & editing. Kathryn Holguin: Investigation, Methodology, Writing – review & editing. Motahareh Mohammadiroudbari: Investigation, Methodology. Chao Luo: Conceptualization, Supervision, Funding acquisition, Writing – original draft, review & editing.

#### *Materials*

Pyromellitic acid (>98%) and hemimellitic acid (>98%) were purchased from TCI and isophthalic acid (99%) was purchased from Alfa Aesar, which are used as received. Tetrasodium benzene-1,2,4,5-tetracarboxylate, trisodium benzene-1,2,3-tricarboxylate, and disodium isophthalate were prepared as follows: pyromellitic acid, hemimellitic acid, or isophthalic acid were dispersed in ethanol with sodium hydroxide powders in 5% excess. The solution was stirred at room temperature for 24 h, then the solution was filtered to collect the precipitate. The precipitate was washed with ethanol and dried in the vacuum oven at 90 °C overnight. The product was a white powder.

### ***Material characterizations***

X-ray diffraction (XRD) pattern was recorded by Rigaku MiniFlex using CuK $\alpha$  radiation; Fourier transform infrared spectroscopy (FTIR) was recorded by Agilent Cary 630 FTIR Spectrometer; Nuclear magnetic resonance (NMR) was recorded by Bruker Ascend 400; SEM images were taken by Hitachi SU-70 analytical ultra-high resolution SEM (Japan).

### ***Electrochemical measurements***

The tetrasodium benzene-1,2,4,5-tetracarboxylate, trisodium benzene-1,2,3-tricarboxylate, or disodium isophthalate was mixed with carbon black and sodium alginate binder to form a slurry at the weight ratio of 60:30:10. The electrode was prepared by casting the slurry onto copper foil using a doctor blade and dried in a vacuum oven at 90 °C overnight. The slurry coated on copper foil was punched into circular electrodes with a mass loading of  $\sim 1.6 \text{ mg cm}^{-2}$ . Coin cells for Na-ion batteries (NIBs) were assembled using sodium metal as the counter electrode, 1 M NaPF<sub>6</sub> in ethylene carbonate/diethyl carbonate (EC/DEC) (1:1 by volume) electrolyte, and glass fiber (Whatman) as the separator. Electrochemical performance was tested using an Arbin battery test station and Landt battery test systems. Cyclic voltammograms (CVs) were recorded using Gamry Reference 1010E Potentiostat/Galvanostat/ZRA with a scan rate of 0.1-2 mV s<sup>-1</sup>. Impedance analysis was also performed by Gamry Reference 1010E Potentiostat/Galvanostat/ZRA.

CVs at various scan rates were used to study the reaction kinetics of Na<sub>4</sub>C<sub>10</sub>H<sub>2</sub>O<sub>8</sub> anode in NIBs. As shown in figure 3a, there is obvious peak separation at 0.1 mV/s, which indicates that the Na<sub>4</sub>C<sub>10</sub>H<sub>2</sub>O<sub>8</sub> anode shows an ion diffusion (intercalation) mechanism. During the discharge/charge process, the Na-ions insert into the Na<sub>4</sub>C<sub>10</sub>H<sub>2</sub>O<sub>8</sub> anode and reversibly react with the two carboxylate groups at the *para* positions of the benzene ring, which is indicated in the

sodiation/de-sodiation mechanism in scheme 1d. In addition, the  $\text{Na}_4\text{C}_{10}\text{H}_2\text{O}_8$  consists of micro-sized particles (1~5  $\mu\text{m}$ ) with numerous nanorods aggregated together, which shows a high specific surface area. Hence, a partial capacitive behavior is exhibited due to monolayer adsorption of ions at the electrode surface.

To conduct the FTIR test before and after cycling, coin cells using  $\text{Na}_4\text{C}_{10}\text{H}_2\text{O}_8$  as the anode and sodium metal as the counter electrode were assembled. After cycling for 1, 10, and 20 cycles at 100  $\text{mA g}^{-1}$ , the coin cells were disassembled in the glovebox. The cycled  $\text{Na}_4\text{C}_{10}\text{H}_2\text{O}_8$  electrodes were washed by DEC and dried in a vacuum oven at 90 °C overnight. Then, the pristine and cycled electrodes were tested by Agilent Cary 630 FTIR Spectrometer. For XRD tests before and after different cycles, thick electrodes were prepared by using polytetrafluoroethylene (PTFE) as a binder to enhance the XRD signal strength. 30 mg  $\text{Na}_4\text{C}_{10}\text{H}_2\text{O}_8$  was mixed with 15 mg carbon black and 5 mg PTFE binder. A thick film was obtained directly after grinding for 20 min. The stainless-steel mesh was used as the current collector. After drying in a vacuum oven at 90 °C overnight, the thick electrodes were assembled in coin cells and cycled for 1, 10 and 20 cycles at 100  $\text{mA g}^{-1}$ . The coin cells were disassembled in glovebox. The cycled electrodes were washed by DEC and dried in a vacuum oven at 90 °C overnight. Then, the pristine and cycled electrodes were tested by Rigaku MiniFlex.

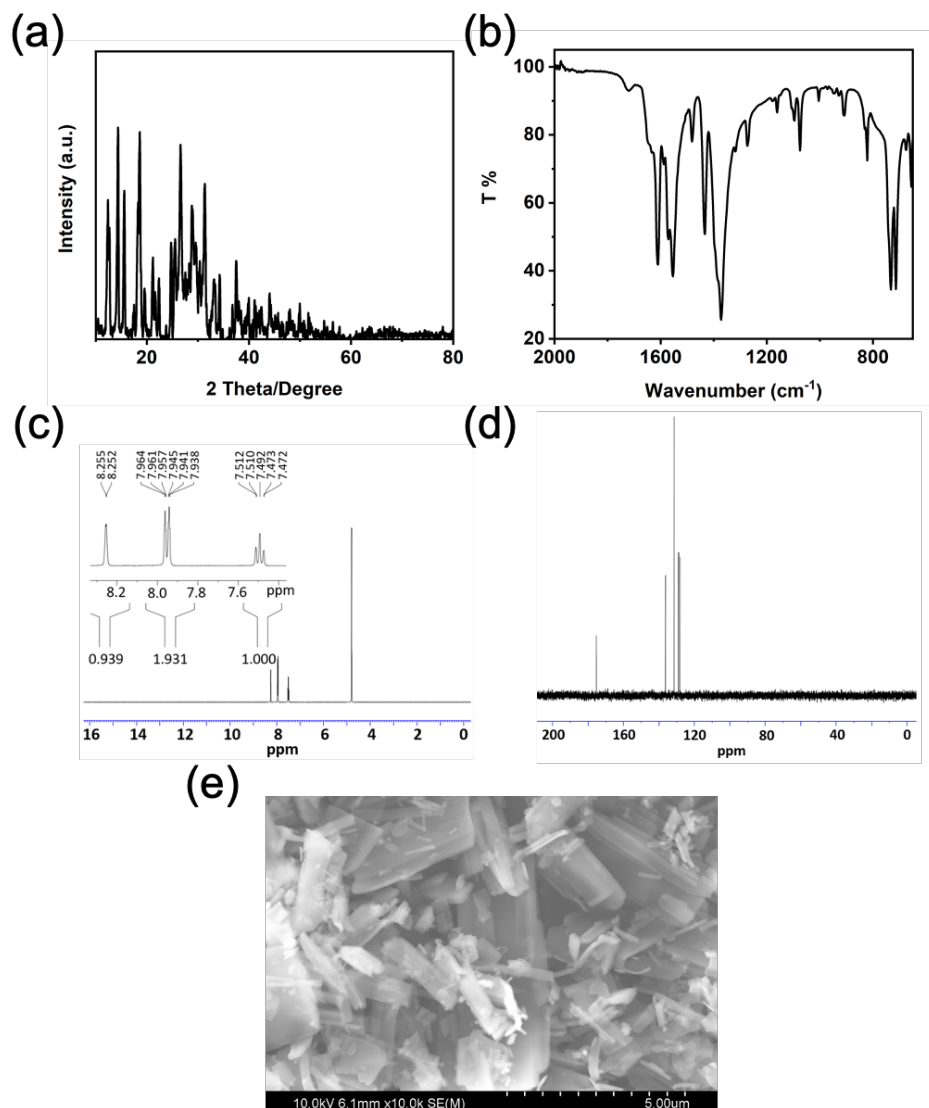


**Figure S1.** Material characterizations for  $\text{Na}_2\text{C}_8\text{H}_4\text{O}_4$ . (a) XRD pattern; (b) FTIR spectrum; (c)  $^1\text{H}$  NMR spectrum; (d)  $^{13}\text{C}$  NMR spectrum; (e) SEM image with a scale of 5  $\mu\text{m}$ .

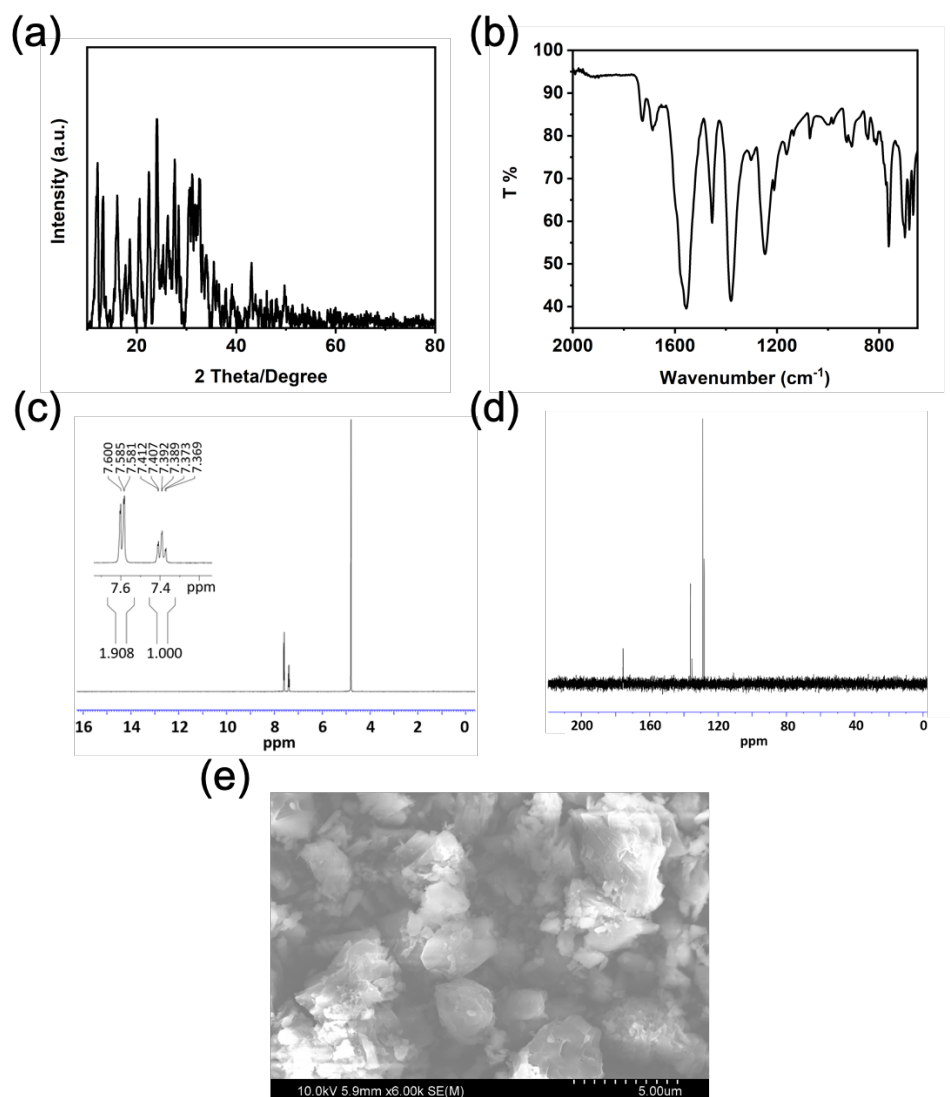


**Figure S2.** Material characterizations for  $\text{Na}_3\text{C}_9\text{H}_3\text{O}_6$ . (a) XRD pattern; (b) FTIR spectrum; (c)  $^1\text{H}$  NMR spectrum; (d)  $^{13}\text{C}$  NMR spectrum; (e) SEM image with a scale of 5  $\mu\text{m}$ .

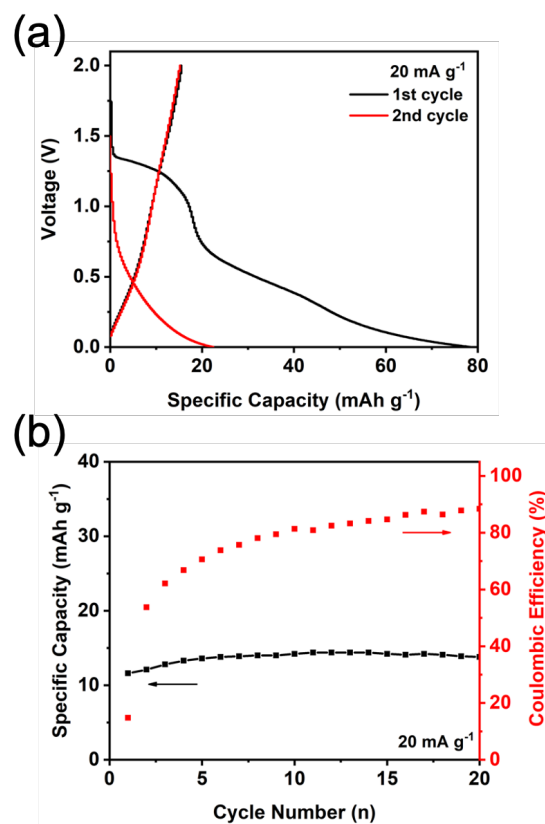


**Figure S3.** Electrochemical performance of  $\text{Na}_2\text{C}_8\text{H}_4\text{O}_4$  in NIBs. (a) Galvanostatic charge-discharge curves; (b) De-sodiation capacity and Coulombic efficiency versus cycle number at the current density of  $20 \text{ mA g}^{-1}$ .

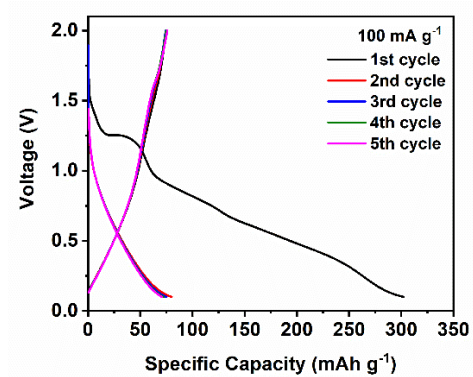


**Figure S4.** Galvanostatic charge-discharge curves of carbon black in NIBs at 100 mA g<sup>-1</sup>.

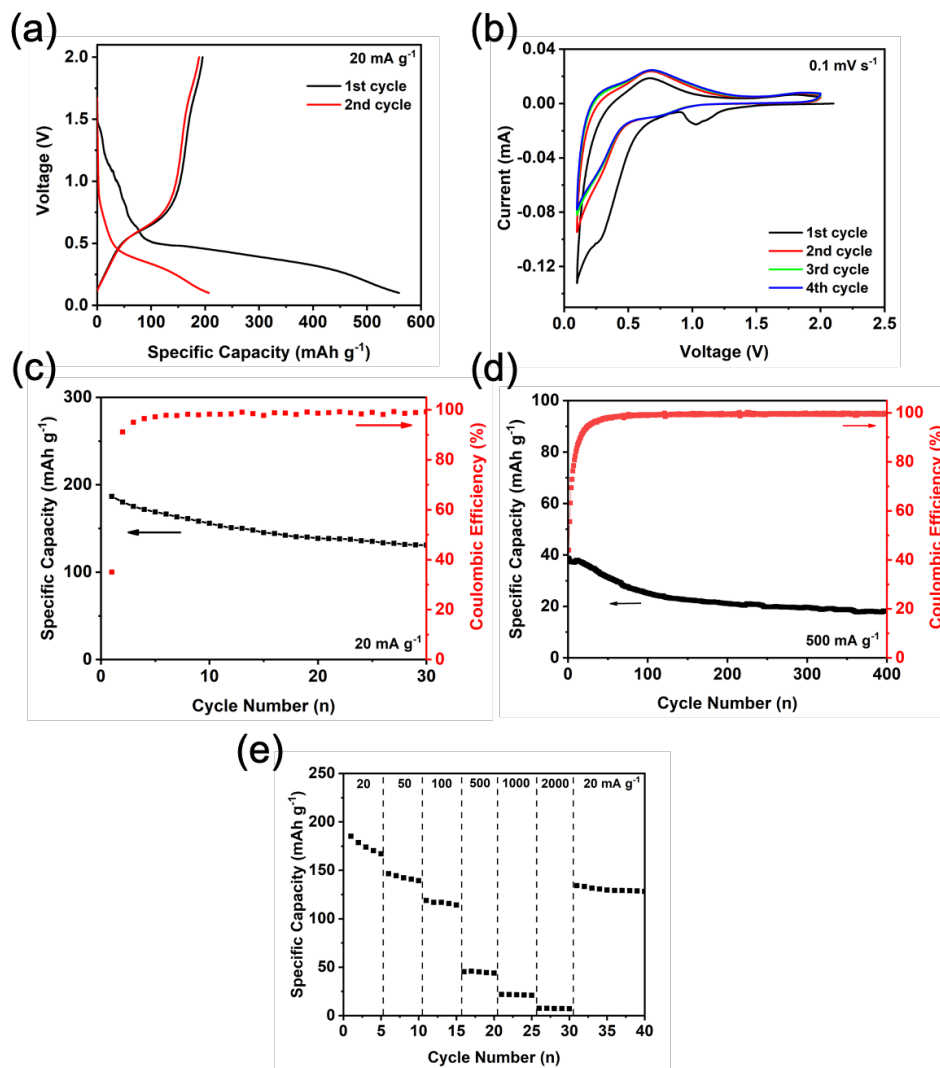


**Figure S5.** Electrochemical performance of  $\text{Na}_3\text{C}_9\text{H}_3\text{O}_6$  in NIBs. (a) Galvanostatic charge-discharge curves; (b) Cyclic voltammograms at  $0.1 \text{ mV s}^{-1}$ ; (c) De-sodiation capacity and Coulombic efficiency versus cycle number at the current density of  $20 \text{ mA g}^{-1}$ ; (d) De-sodiation capacity and Coulombic efficiency versus cycle number at the current density of  $500 \text{ mA g}^{-1}$ ; (e) Rate performance at various current densities.